REVISTA INTERDISCIPLINAR DE PESQUISA EM ENGENHARIA

CILAMCE 2016

XXXVII IBERIAN LATIN AMERICAN CONGRESS ON COMPUTATIONAL METHODS IN ENGINEERING
BRASÍLIA - DF - BRAZIL

PARAMETRIC OPTIMIZATION OF A PIEZOELECTRIC ACTUATOR BONDED TO AN ISOTROPIC THIN PLATE

Juliano F. Gonçalves

Tales V. Lisbôa

Filipe P. Geiger

juliano.fagundes@ufrgs.br

taleslisboa@daad-alumni.de

filipe.geiger@ufrgs.br

Department of Mechanical Engineering, Federal University of Rio Grande do Sul - UFRGS

R. Sarmento Leite 425, CEP 90050-170, Porto Alegre, Brazil

Daniel M. De Leon

daniel.leon@furg.br

School of Engineering, Federal University of Rio Grande - FURG

Av. Itália Km 8, Campus Carreiros, CEP 96203-900, Rio Grande, Brazil

Abstract. *This paper presents a parametric optimization procedure in order to obtain the best position of an actuator bonded to a thin plate. The semi-analytical static response is determined by means of the pb-2 Rayleigh-Ritz Method. The design parameters for the optimization problem are chosen as the position (2-D) and the orientation of a rectangular shaped actuator. The electric-mechanical coupling influence is represented as mechanical forces applied to the plate's reference surface. The main objective of this work is to find the optimal design sets which would produce a mechanical loading condition that minimizes the transverse displacement of a given point in the plate. The methodology is applied and solutions are obtained for several boundary plate conditions.*

Keywords: *thin plates, parametric optimization, piezoelectric actuators*

1 INTRODUCTION

The field of smart materials and structures has raised during the last decades. Unlike conventional structures, which are passive, this kind of systems have the ability to change its properties or configuration during the operation. Applications involve vibration control, shape control, health monitoring, energy harvesting, etc.

In order to find better positions and/or shapes for the actuators, optimization procedures might be employed. Liew et al., (2002), presented a formulation by employing the Element-Free Galerkin method based on the first-order shear deformation theory to study the shape control of laminated composite plates with piezoelectric patches. Nguyen & Tong, (2004), addressed the problem of static deformation of smart composite plate structures by means of a finite element formulation with non-rectangular shaped actuators. A numerical investigation was carried out to find the influence of the actuator pattern on the shape match factor and a given voltage. Sun & Tong, (2005), studied the static shape control of smart plate structures using piezoelectric actuator patches. The optimization problem was defined as the minimization of the number of piezoelectric patches and their respective control voltages in order to minimize the energy spent to control the system.

The *pb-2* Rayleigh-Ritz Method (*pb-2* RRM) is used to approximate the solution of the differential equations. This method works successfully for solving plate equilibrium equations. It interpolates the problem solution by weighted kinematically admissible functions. The modification, namely *pb-2*, eases the kinematic requirement by multiplying the entire basis by beam functions, or Bhat's functions (Bhat, 1985), which represents the plate's edges. Exponents of these monomials defines the plate's boundary conditions, facilitating the consideration of any kind of boundary conditions set. The solutions obtained by RRM have a semi-analytical construction, hence easing the attempt of derivatives determination. Liew & Wang, (1993), applied the method to study the transverse displacement and bending moments of plates under lateral loading. Liew et al., (1993), analysed free vibrations in thick plates with several boundary conditions while Singh & Elahabash, (2003), derived the equilibrium path using quadrangular thin plates under lateral loading for large displacements.

In this work, we intend to find the optimum placement and orientation of a piezoelectric patch which would reduce the static displacement for a given point in a thin plate. This is a preliminary approach aiming to establish an optimization procedure using a semi-analytical response and, henceforth, extending this scheme to control structures using more complex shapes for the actuators.

A conjugate gradient scheme is applied to the optimization problem and, as the actuator's influence is restricted to the external forces, the derivatives necessary to perform the gradient search are only concerned to the external potential. As stated before, the derivatives are taken analytically.

Both matrix and index notation are used throughout the text. Greek index varies from 1 to 2 as well as small-caps Arabic index varies from 1 to 3. Other indices vary according the to text. This paper is composed by five sections. The first one describes the governing equations of thin plates theory. The second section presents the application of the *pb-2* RRM in these equations. The third section details the parametric optimization. Numerical results are described in section four. The section five is the conclusion remarks.

2 THIN PLATE THEORY

The displacement field of a thin plate (Fig. 1) in bending is written as (Dym & Shames, 2013):

$$\begin{aligned} u_1(x_1, x_2, x_3) &= -x_3 u_{3,1}(x_1, x_2) \\ u_2(x_1, x_2, x_3) &= -x_3 u_{3,2}(x_1, x_2) \\ u_3(x_1, x_2) &= u_3(x_1, x_2) \end{aligned} \tag{1}$$

where u_α and u_3 are the membrane and transverse displacements, respectively, and x_i are the Cartesian coordinate axes. In Figure 1, $\mathbf{F}$ denotes an applied force to the upper plate's surface while $\mathbf{M}$ corresponds to the respective moment with respect to the reference surface, which is represented by the crosshatch area Λ. The outwards vector on $\partial\Lambda$ (the boundary of Λ) is defined by $\mathbf{n}$, while Ω is the plate's domain and q illustrates the lateral loading.

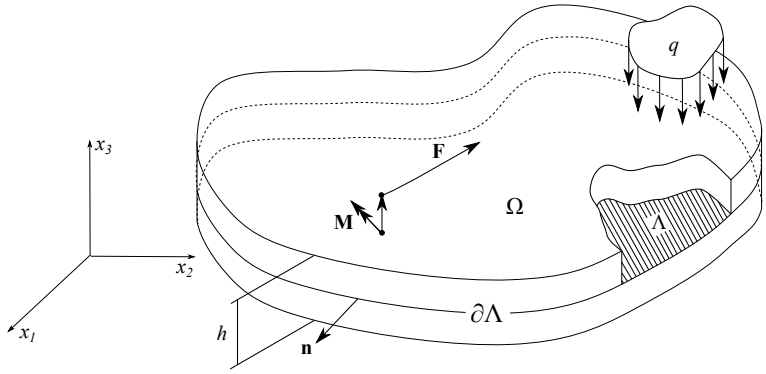

Figure 1: Applied loading and boundary conditions for the plate.

The right side of Eq. (1) shows a dependence only on x_1 and x_2 axes, while the dependence on x_3 is explicit. For the sake of simplicity, the dependence of u_3 on x_1 and x_2 will be omitted. Moreover, membrane displacements are neglected due to the decoupling between them and the transverse displacements, for homogeneous plates.

The strain ($\boldsymbol{\varepsilon}$) and stress ($\boldsymbol{\sigma}$) vectors are defined, respectively, as:

$$\boldsymbol{\varepsilon} = -x_3 \boldsymbol{\kappa} \qquad \boldsymbol{\sigma} = \hat{\mathbf{C}}\boldsymbol{\epsilon} = -x_3 \hat{\mathbf{C}}\boldsymbol{\kappa} \tag{2}$$

where:

$$\boldsymbol{\kappa} = \begin{Bmatrix} u_{3,11} & u_{3,22} & 2u_{3,12} \end{Bmatrix}^{\mathrm{T}} \tag{3}$$

and:

$$\hat{\mathbf{C}} = \begin{bmatrix} \hat{C}_{11} & \hat{C}_{12} & 0 \\ & \hat{C}_{11} & 0 \\ sym & & \frac{1}{2}\left(\hat{C}_{11} - \hat{C}_{12}\right) \end{bmatrix} \tag{4}$$

It is well-known in plate's theory that $\boldsymbol{\kappa}$ is a vector with the plate's curvatures. The matrix $\hat{\mathbf{C}}$ denotes the isotropic reduced constitutive tensor.

The equivalent stresses are defined by the integration of the stresses over the thickness. Due to the plate's homogeneity, normal equivalent stresses are decoupled from the curvature effects, resulting in (Reddy, 2007):

$$\mathbf{M} = \begin{Bmatrix} M_{11} & M_{22} & M_{12} \end{Bmatrix}^{\mathrm{T}} = \int_{\frac{-h}{2}}^{\frac{-h}{2}} x_3 \boldsymbol{\sigma} \mathrm{d}x_3 = -\mathbf{D}\boldsymbol{\kappa} \tag{5}$$

where M_{11} and M_{22} correspond to the bending moments, M_{12} is the twisting moment and $\mathbf{D} = \hat{\mathbf{C}}h^3/12$ denotes the plate stiffness.

Applying Eq. (5) into the equilibrium equations together with Eq. (2), one can derive the equilibrium equations of a thin plate in bending in terms of the transverse displacement u_3 as:

$$D_{11}\left(\frac{\partial^4}{\partial x_1^4} + \frac{\partial^4}{\partial x_1^2 \partial x_2^2} + \frac{\partial^4}{\partial x_2^4}\right) u_3 = F \qquad \therefore \qquad D_{11}\boldsymbol{\nabla}^2 u_3 = F \tag{6}$$

where $\boldsymbol{\nabla}^2$ is the bi-harmonic operator and F is the lateral loading. Equation (6) is subjected to three types of boundary conditions:

$$\begin{aligned} &\bullet \text{ Clamped Edge (C):} && u_3(x_1, x_2) = 0 \;\; \& \;\; \frac{\partial u_3(x_1, x_2)}{\partial \mathbf{n}} = 0 \\ &\bullet \text{ Simply-Supported Edge (S):} && u_3(x_1, x_2) = 0 \;\; \& \;\; M_{\mathbf{nn}} = 0 \\ &\bullet \text{ Free Edge (F):} && M_{\mathbf{nn}} = 0 \;\; \& \;\; V_{\mathbf{n}} = 0 \end{aligned} \tag{7}$$

where V is the equivalent shear stress. These boundary conditions must be satisfied in each edge of the plate. Considering the analysis proposed, F is composed by distributed transverse loadings and applied moments which comes from the piezoelectric actuators, as it will be seen in the next section.

3 ACTUATOR MODELING

In this work, the piezoelectric actuator is considered as bonded to the upper surface of the plate, which is the usual application of Macro Fiber Composite (MFC). The MFC is a

piezoelectric composite actuator and consists of a plane array of piezo ceramic rods sandwiched between layers of adhesive, electrodes and polyimide film (High and Wilkie, 2003).

Although there is a coupling between the mechanical and electrical fields, we used a simplified model to represent the interaction between the MFC and the plate structure. Padoin et al. (2015) employed a similar approach in order to avoid the assembly of an electromechanical coupling matrix to model a plate structure with bonded MFC through finite element method. In order to simplify the analysis, the acting forces are divided into four points, as shown in Fig. 2.

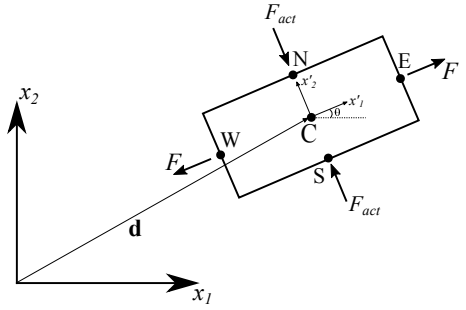

Figure 2: Simplified model to represent the interaction between the MFC and the plate structure.

As a result, the actuator influence over the plate is considered as forces applied to the upper-surface of the plate which are transferred to the mid-surface as bending moments. The membrane forces are ignored given the decoupling between the membrane and bending effects. Bending moments are applied in the points E, N, W and S and they are written as:

$$\begin{aligned} \mathbf{M}^{(E)} &= \frac{Fh}{2}\begin{Bmatrix} -\sin\theta \\ \cos\theta \end{Bmatrix} & \mathbf{M}^{(N)} &= \frac{F_{act}h}{2}\begin{Bmatrix} \sin\theta \\ \cos\theta \end{Bmatrix} \\ \mathbf{M}^{(W)} &= \frac{Fh}{2}\begin{Bmatrix} \sin\theta \\ -\cos\theta \end{Bmatrix} & \mathbf{M}^{(S)} &= \frac{F_{act}h}{2}\begin{Bmatrix} -\sin\theta \\ -\cos\theta \end{Bmatrix} \end{aligned} \tag{8}$$

where F is the actuator's applied load.

Usually, the actuator has a main direction. By Poisson effect, forces perpendicular to this main direction may appear. As a result, if the electric potential expands the actuator in one direction (applying tension forces to the plate), it contracts in the other (applying contraction forces to the plate), these two forces are described by F and F_{act}, respectively.

4 *PB-2* RAYLEIGH-RITZ METHOD

The *Pb-2* Rayleigh-Ritz is a variational method used to approximate the thin plate's displacement field by kinematically admissible functions in which weights are determined by the minimization of the total potential functional. This functional is composed by both the strain energy and the external potential, and they must be defined in terms of displacements.

The strain energy, U_{int}, is derived as:

$$U_{\text{int}} = \frac{1}{2}\int_{\Omega} \boldsymbol{\sigma}^{\mathrm{T}}\boldsymbol{\varepsilon}\ \mathrm{d}\Omega = \frac{1}{2}\int_{\Omega} x_3^2\boldsymbol{\kappa}^{\mathrm{T}}\hat{\mathbf{C}}\boldsymbol{\kappa}\ \mathrm{d}\Omega = \frac{1}{2}\int_{\Lambda} \boldsymbol{\kappa}^{\mathrm{T}}\mathbf{D}\boldsymbol{\kappa}\ \mathrm{d}\Lambda \tag{9}$$

The external potential, U_{ext}, is derived as:

$$U_{\text{ext}} = -\int_{\Lambda} q u_3 \, \mathrm{d}\Lambda - \sum_{k=1}^{N} M_{\omega}^{(k)} \frac{\partial u_3}{\partial x_{\omega}}\bigg|_{\mathbf{x}=\mathbf{x}^{(N)}} \tag{10}$$

where ω does not sum and denotes the axis in which the moment is applied, q corresponds to the lateral loading acting over the plate's mid-surface and $M_{\omega}^{(k)}$ are the applied moments, due to the actuator expansion/contraction. The vector $\mathbf{x}^{(N)}$ contains the cartesian coordinates of the moment (E, N, W and S points, see Fig. 2).

The displacement field is approximate by a set of functions as:

$$u_3 = \boldsymbol{\phi}^{\mathrm{T}} \boldsymbol{\lambda} \tag{11}$$

where $\boldsymbol{\phi}$ and $\boldsymbol{\lambda}$ are vectors corresponding to kinematically admissible interpolation functions and weighting constants, respectively. Since the monomials multiply the approximation basis and in order to ease the quadrature process, polynomials are chosen as interpolation functions.

Therefore, $\boldsymbol{\phi}$ is written as:

$$\phi_r = G\left(x_1, x_2\right) x_1^{(i-1)} x_2^{(l-i-1)} \qquad r = \frac{(l+1)\,(l+2)}{2} - i \qquad 1 \leq r \leq m \tag{12}$$

where i and l are counters, r corresponds to the position of the function in $\boldsymbol{\phi}$, m denotes the span size and G are the Bhat's functions:

$$G\left(x_1, x_2\right) = \left(\Theta_1\left(x_1, x_2\right)\right)^{g_1} \left(\Theta_2\left(x_1, x_2\right)\right)^{g_2} \left(\Theta_3\left(x_1, x_2\right)\right)^{g_3} \left(\Theta_4\left(x_1, x_2\right)\right)^{g_4} \tag{13}$$

where g_I, $I = 1..4$, are integers corresponding to the boundary conditions (Eq. (7)). For rectangular plates, the beam functions are written as:

$$\Theta_1 = x_2 \qquad \Theta_2 = x_1 - a \qquad \Theta_3 = x_2 - b \qquad \Theta_4 = x_1 \tag{14}$$

The strain energy and external potential are defined as:

$$\begin{aligned} U_{\text{int}} &= \frac{1}{2}\boldsymbol{\lambda} \int_{\Lambda} \mathbf{N}^{\mathrm{T}} \mathbf{D} \mathbf{N} \, \mathrm{d}\Lambda \boldsymbol{\lambda} \\ U_{\text{ext}} &= -\int_{\Lambda} q \boldsymbol{\phi}^{\mathrm{T}} \, \mathrm{d}\Lambda \, \boldsymbol{\lambda} - \left[\sum_{k=1}^{N} M_{\alpha}^{(k)} \frac{\partial \boldsymbol{\phi}^{\mathrm{T}}}{\partial x_{\alpha}}\bigg|_{\mathbf{x}=\mathbf{x}^{(N)}} \boldsymbol{\lambda} \right] \end{aligned} \tag{15}$$

The total potential functional is defined as the sum of the strain energy and the external potential. In the Rayleigh-Ritz Method, the variation is produced over the weighting constants, resulting in:

$$\Pi = U_{\text{int}} + U_{\text{ext}} \qquad \delta\Pi = 0 \quad \therefore \quad \frac{\partial U_{\text{int}}}{\partial \boldsymbol{\lambda}} + \frac{\partial U_{\text{ext}}}{\partial \boldsymbol{\lambda}} = \mathbf{0} \tag{16}$$

which can be described as:

$$\begin{aligned} \mathbf{P}\boldsymbol{\lambda} &= \frac{\partial U_{\text{int}}}{\partial \boldsymbol{\lambda}} = \int_{\Lambda} \mathbf{N}^{\mathrm{T}}\mathbf{D}\mathbf{N} \, \mathrm{d}\Lambda \, \boldsymbol{\lambda} \\ \mathbf{w} &= \frac{\partial U_{\text{ext}}}{\partial \boldsymbol{\lambda}} = \int_{\Lambda} q\boldsymbol{\Phi}^{\mathrm{T}} \, \mathrm{d}\Lambda + \left[\sum_{k=1}^{N} M_{\alpha}^{(k)} \frac{\partial \boldsymbol{\phi}^{\mathrm{T}}}{\partial x_{\alpha}} \bigg|_{\mathbf{x}=\mathbf{x}^{(N)}} \right] \end{aligned} \tag{17}$$

which results in a linear system:

$$\mathbf{P}\boldsymbol{\lambda} = \mathbf{w} \tag{18}$$

5 PARAMETRIC OPTIMIZATION

The optimization problem is written as the transverse displacement minimization of a given point in the plate. Side constraints are included in the formulation aiming to guarantee the actuator will be placed inside the physical plate domain. Since these constraints are non-differentiable, they must be verified in each iteration loop. In a standard form, this problem can be written as:

$$\min_{\boldsymbol{\rho}} \quad f = u_3^{pos} \tag{19}$$

$$\text{subject to} \begin{cases} 0.1 \leq x_1 \leq 0.9 \\ \\ 0.1 \leq x_2 \leq 0.9 \end{cases} \tag{20}$$

where u_3^{pos} is the target transverse displacement. The limits for x_1 and x_2 were chosen considering the actuator dimensions.

The design variables for the optimization problem are the actuator coordinates and orientation:

$$\boldsymbol{\rho}^{(0)} = \left\{ x_1^{(0)} \quad x_2^{(0)} \quad \theta^{(0)} \right\}^{\mathrm{T}} \tag{21}$$

The conjugate gradient method is applied to the optimization problem (Arora, 2004). Considering Eq. (21) as an initial guess, the gradient is determined in the first step as:

$$\mathbf{g}^{(0)} = -\boldsymbol{\nabla} u_3(\boldsymbol{\rho}^{(0)}) \tag{22}$$

where $\boldsymbol{\nabla}$ is a first-order differential operator with respect to the design variables. The next set of design variables is determined by:

$$\boldsymbol{\rho}^{(k+1)} = \boldsymbol{\rho}^{(k)} + \alpha \mathbf{g}^{(k)} \tag{23}$$

where α is the step size which was chosen *a priori*.

Since the first step is computed, the next conjugate directions are modified to:

$$\mathbf{g}^{(k)} = -\boldsymbol{\nabla} u_3(\boldsymbol{\rho}^{(k)}) + \beta^{(k)} \mathbf{g}^{(k-1)} \tag{24}$$

where:

$$\beta^{(k)} = \left[\frac{||\boldsymbol{\nabla} u_3(\boldsymbol{\rho}^{(k)})||}{||\boldsymbol{\nabla} u_3(\boldsymbol{\rho}^{(k-1)})||} \right]^{1/2} \tag{25}$$

where $||\cdot||$ denotes the norm of the vector.

The stop criteria is defined by:

$$||\boldsymbol{\nabla} u_3(\boldsymbol{\rho}^{(k)})|| < \epsilon \tag{26}$$

which ϵ is a small tolerance.

Considering that *pb-2* RRM generates semi-analytical solutions, the derivatives computation is a straightforward process. Moreover, as design variables affect only the external potential, none differentiation is need to $\mathbf{P}$. Therefore, the gradient of the transverse displacement is written as:

$$\boldsymbol{\nabla} u_3 = \boldsymbol{\nabla} \left(\boldsymbol{\phi}^{\mathrm{T}} \boldsymbol{\lambda} \right) \rightarrow \nabla_s u_3 = \nabla_s \left(\sum_{n=1}^{K} \phi_n \lambda_n \right) = \sum_{n=1}^{K} \phi_n \nabla_s \lambda_n \tag{27}$$

resulting in:

$$\boldsymbol{\nabla} u_3 = \left(\boldsymbol{\lambda}^{\mathrm{T}} \otimes \boldsymbol{\nabla} \right) \boldsymbol{\phi} \quad \therefore \quad \boldsymbol{\nabla} u_3 = \left(\boldsymbol{\nabla} \otimes \mathbf{w}^{\mathrm{T}} (\boldsymbol{\rho}) \right) \mathbf{P}^{-\mathbf{1}} \boldsymbol{\phi} \tag{28}$$

where $\otimes$ corresponds to the dyadic product.

6 NUMERICAL RESULTS

The optimization procedure was employed to find the actuator's position and orientation which minimizes the displacement of a given point. Four cases were analyzed considering different boundary conditions, as presented in Table 1 with the circle representing the point where the displacement is minimized (u_3^{pos}).

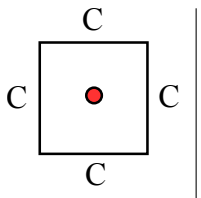	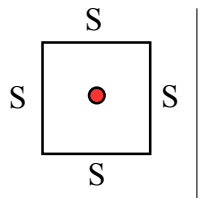	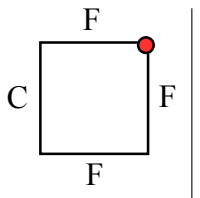	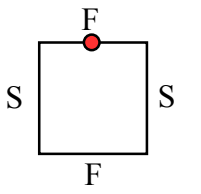
$q = 15\ \mathrm{N/m^2}$	$q = 10\ \mathrm{N/m^2}$	$q = 5\ \mathrm{N/m^2}$	$q = 10\ \mathrm{N/m^2}$
(a) CCCC	(b) SSSS	(c) CFFF	(d) SFSF

Table 1: Cases analyzed and assessed positions.

The plate dimensions are $1 \times 1 \times 0.01$ m. The plate's elastic properties are defined by $E = 200.10^9$ GPa and $\nu = 0.3$, where E and ν denote the Young's modulus and the Poisson's ratio, respectively. The lateral loading is uniform and applied over the entire reference surface and its value varies from case to case and is presented in Table 1. The actuator force F is considered as 300 N, as a result of applying approximately 1000 V to the aforementioned actuator's electrodes.

Moreover, due to the Poisson's effect, a perpendicular force is applied as well (Fig. 2), 93 N ($\nu_{act} = 0.31$). In all cases, $m = 20$ for the span size of RRM basis, which corresponds to 231 constants. Such a high value is necessary in order to analyze the actuator local effects over the plate properly . For all cases, three different initial positions are considered, namely ρ^a, ρ^b and ρ^c:

$$\rho^a = \begin{Bmatrix} 0.6 & 0.4 & 20 \end{Bmatrix}^{\mathrm{T}} \qquad \rho^b = \begin{Bmatrix} 0.25 & 0.45 & 10 \end{Bmatrix}^{\mathrm{T}} \qquad \rho^c = \begin{Bmatrix} 0.75 & 0.8 & 80 \end{Bmatrix}^{\mathrm{T}} \tag{29}$$

In the results presentation, the centre plate displacement is normalized as well as the actuator's orientation by:

$$\hat{u}_3 = \frac{u_3^{\mathrm{pos}} D_{11}}{q a^4} \qquad \hat{\theta} = \frac{\theta}{90}\ [^\circ] \tag{30}$$

In the following subsections, results for the four test cases are presented.

6.1 Case (a) CCCC

Figure 3 shows the objective function convergence and the evolution of the design variables during the optimization process.

It can be seen from Fig.3(a) that whichever the starting point, the objective function converges to the same value. However, different final positions are found for the three starting points, as shown in Figure 4.

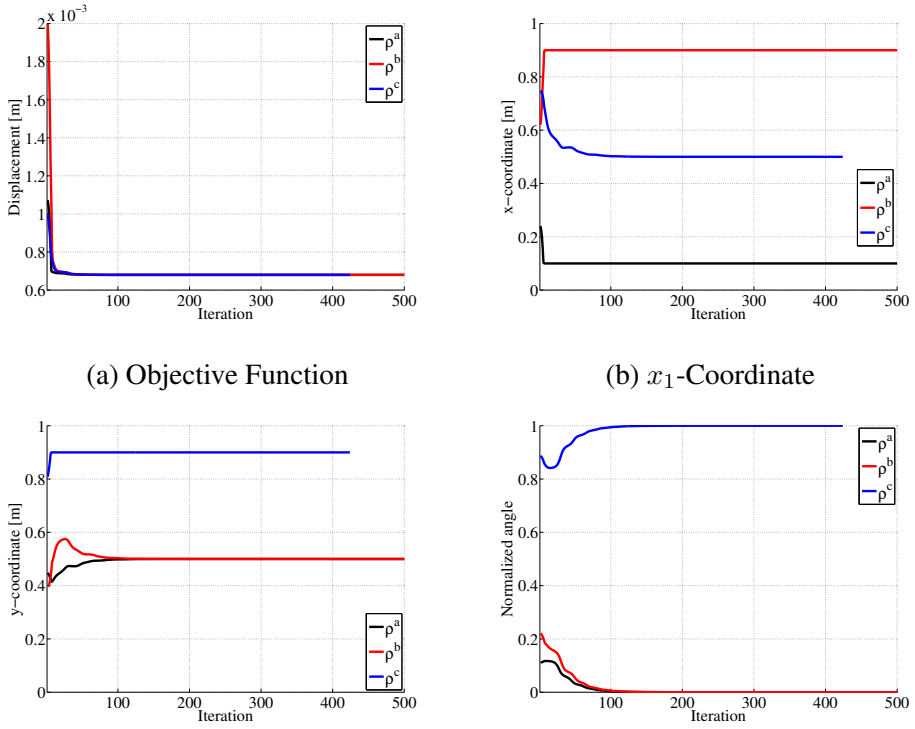

(a) Objective Function

(b) x_1-Coordinate

(c) x_2-Coordinate

(d) Normalized Angle

Figure 3: Objective function convergence and design variables history for CCCC.

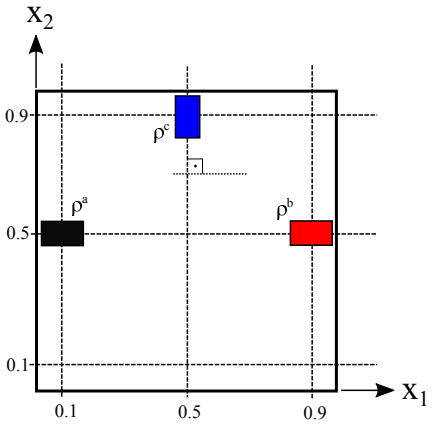

Figure 4: Illustration of the optimized designs for case (a) CCCC.

6.2 Case (b) SSSS

For the second example, it can be seen that the three starting points converge to the same minimum (Fig. 5).

The same behavior occurs for this test case, where the different final positions relies on the boundary conditions, as shown in Figure 6.

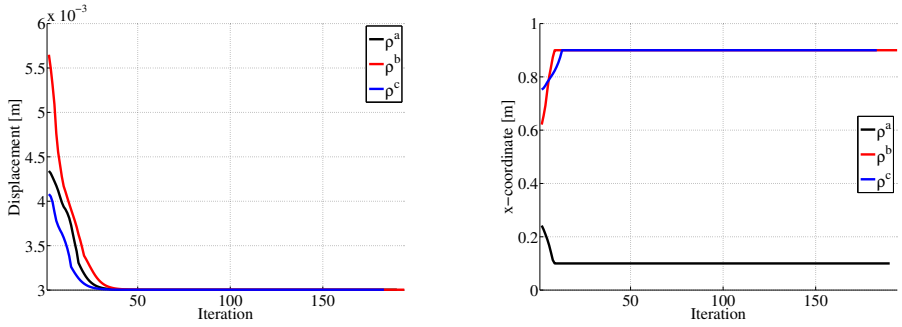

(a) Objective Function

(b) x_1-Coordinate

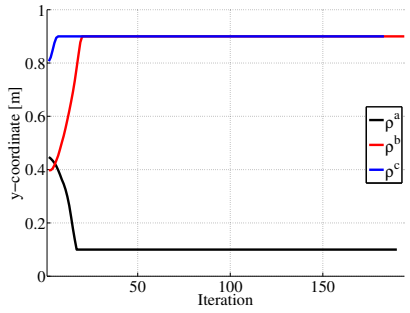

(c) x_2-Coordinate

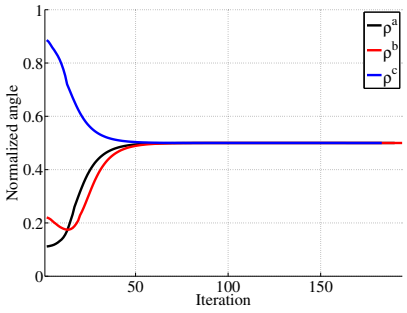

(d) Normalized Angle

Figure 5: Objective function convergence and design variables history for SSSS.

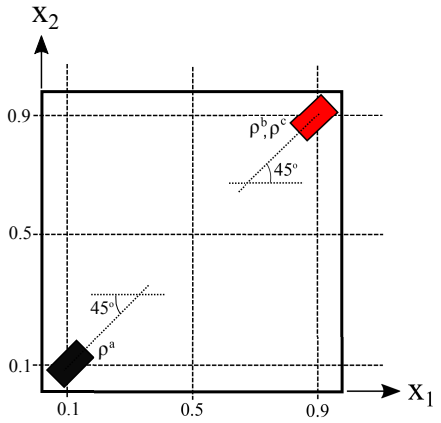

Figure 6: Illustration of the optimized designs for case (b) SSSS.

6.3 Case (c) CFFF

This test case is slightly different from the previous examples since there is only one axis of symmetry due to the imposed boundary conditions. This condition combined to the position where the displacement is minimized resulted in a poor local minima for one of the initial guesses, as can be seen in Fig. 7.

6.4 Case (d) SFSF

For this test case, the same behavior is observed where a local minimum is found which highlights the importance of the initial guesses for non-symmetric problems.

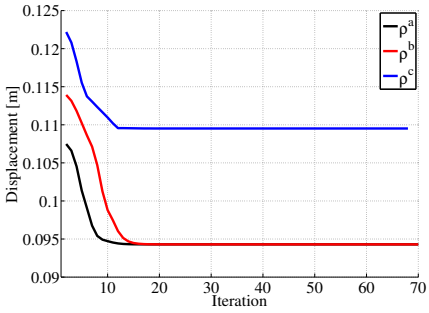

(a) Objective Function

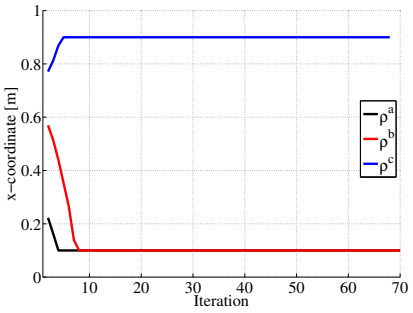

(b) x_1-Coordinate

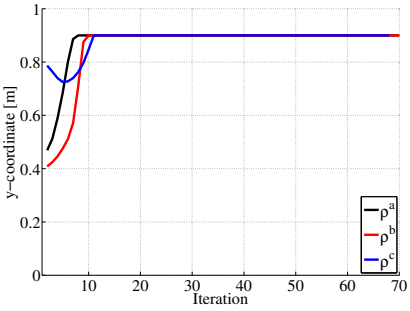

(c) x_2-Coordinate

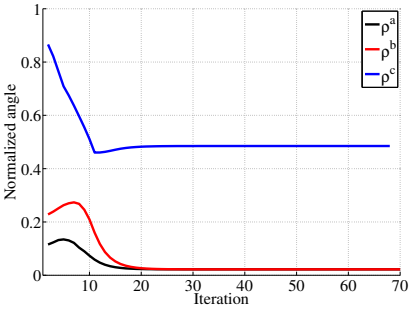

(d) Normalized Angle

Figure 7: Objective function convergence and design variables history for CFFF.

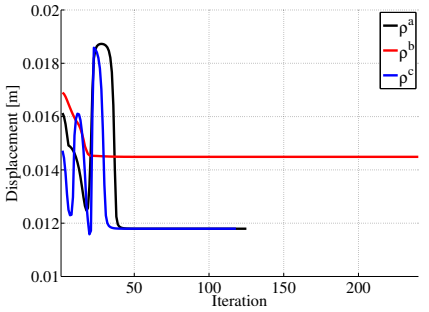

(a) Objective Function

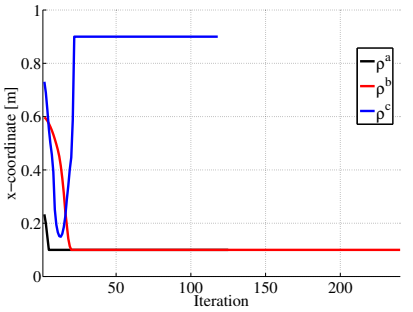

(b) x_1-Coordinate

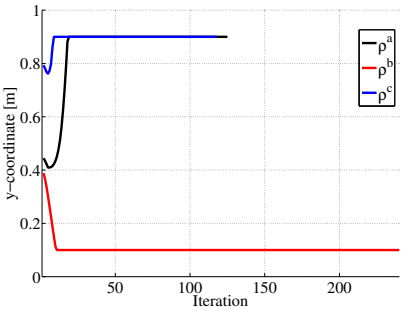

(c) x_2-Coordinate

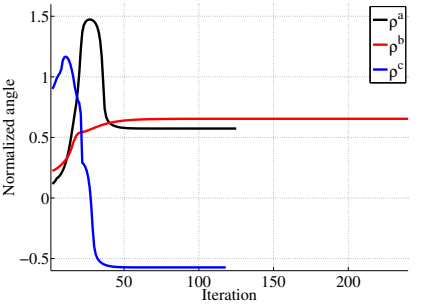

(d) Normalized Angle

Figure 8: Objective function convergence and design variables history for SFSF.

7 CONCLUSIONS

This work presents a parametric optimization procedure to find the optimal configuration of a piezoelectric actuator bonded to a thin plate. Although simple test cases were carried out, the preliminary numerical results obtained for the four cases demonstrate the effectiveness of this methodology. The transverse displacement of a point of the plate is considered as objective function. A semi-analytical static response is found by means of the *Pb-2* Rayleigh-Ritz method, and the sensitivities with respect to the design variables are straightforward obtained. Local minima were found for the test cases with non-symmetrical boundary conditions. In the authors point of view, the local strain generated by the actuator might be responsible for this issue. As could be seen in these particular test cases, for some starting points the optimization process leads to a very poor local minimum. However, it can be overcome by multi-start execution techniques. The results presented in this work, as well as the optimization formulation constitutes a preliminary investigation towards more complex problems, as the actuator shape optimization problem, for instance. It is the next natural step of the problem aiming the plate control by piezoelectric actuators.

REFERENCES

Arora, J. S., 2004. *Introduction to optimum design*, Elsevier, UK.

Bhat, R. B., 1985. Plate Deflections using Orthogonal Polynomials. *Journal of Engineering Mechanics*, **111(11)**:1301–1309.

Dym, C. L., & Shames, I. H. 2013. *Solid Mechanics: A Variational Approach. Augmented Edition* Springer Science+Business Media, New York.

High, J. W. & Wilkie, W. K., 2003. Method of fabricating NASA-standard macro-fiber composite piezoelectric actuators.

Liew, K. M., & Lim, H. K., Tan, M. J., & He, X. Q., 2002. Analysis of laminated composite beams and plates with piezoelectric patches using the element-free Galerkin method. *Computational Mechanics*, vol. 29, n. 6, pp. 486-497.

Liew, K. M., & Wang, C. M., 1993. *pb-2* Rayleigh-Ritz Method for General Plate Analysis, *Engineering Structures*, **15(1)**:55–60.

Liew, K. M., & Xiang, Y., Kitipornchai, S, 1993. Transverse Vibration of Thick Rectangular Plates-I. Comprehensive Sets of Boundary Conditions, *Computers & Structures*, **49(1)**:1–29.

Nguyen, Q., & Tong, L., 2004. Shape control of smart composite plate with non-rectangular piezoelectric actuators. *Composite structures*, vol. 66, n. 1, pp. 207-214.

Padoin, E., Fonseca, J. S. O., Perondi, E. A., & Menuzzi, O., 2015. Optimal placement of piezoelectric macro fiber composite patches on composite plates for vibration suppression. *Latin American Journal of Solids and Structures*, vol. 12, n. 5, pp. 925-947.

Reddy, J. N., 2007. *Theory and Analysis of Elastic Plates and Shells*, CRC Press, Boca Raton.

Singh, A. V., & Elaghabash, Y., 2003. On Finite Displacement Analysis of Quadrangular Plates, *International Journal of Non-Linear Mechanics*, *38(8)*:1149–1162.

Sun, D., & Tong, L., 2005. Design optimization of piezoelectric actuator patterns for static shape control of smart plates. *Smart materials and structures*, vol. 14, n. 6, pp. 1353.